Low Band-Gap D–A Conjugated Copolymers Based on Anthradithiophene and Diketopyrrolopyrrole for Polymer Solar Cells and Field-Effect Transistors

Jun Huang, Yongxiang Zhu, Lianjie Zhang, Ping Cai, Xiaofeng Xu, Junwu Chen, Yong Cao

Institute of Polymer Optoelectronic Materials & Devices, State Key Laboratory of Luminescent Materials & Devices, South China University of Technology, Guangzhou 510640, People's Republic of China

Correspondence to: L. Zhang (E-mail: lianjiezhang@scut.edu.cn) or J. Chen (E-mail: psjwchen@scut.edu.cn)

Received 27 January 2014; accepted 11 March 2014; published online 25 March 2014

DOI: 10.1002/pola.27163

ABSTRACT: Two conjugated copolymers PADT-DPP and PADT-FDPP based on anthradithiophene and diketopyrrolopyrrole, with thiophene and furan as the π-conjugated bridge, respectively, were successfully synthesized and characterized. The number-averaged molecular weights of the two polymers are 38.7 and 30.2 kg/mol, respectively. Polymers PADT-DPP and PADT-FDPP exhibit broad absorption bands and their optical band gaps are 1.44 and 1.50 eV, respectively. The highest occupied molecular orbital energy level of PADT-DPP is located at -5.03 eV while that of PADT-FDPP is at -5.16 eV. In field-effect transistors, PADT-DPP and PADT-FDPP displayed hole mobilities of 4.7×10^{-3} and 2.7×10^{-3} cm^2/(V s), respectively. In polymer solar cells, PADT-DPP and PADT-FDPP showed power conversion efficiency (PCE) of 3.44% and 0.29%, respectively. Atomic force microscopy revealed that the poor efficiency of PADT-FDPP should be related to the large two-phase separation in its active layer. If 1,8-diiodooctane (DIO) was used as the solvent additive, the PCE of PADT-DPP remained almost unchanged due to very limited morphology variation. However, the addition of DIO could remarkably elevate the PCE of PADT-FDPP to 2.62% because of the greatly improved morphology. Our results suggest that the anthradithiophene as an electron-donating polycyclic system is useful to construct new D–A alternating copolymers for efficient polymer solar cells. © 2014 Wiley Periodicals, Inc. J. Polym. Sci., Part A: Polym. Chem. **2014**, *52*, 1652–1661

KEYWORDS: anthradithiophene; charge transport; conjugated polymers; diketopyrrolopyrrole; macrocycles; polymer solar cells

INTRODUCTION The development of low band-gap conjugated polymer donor plays an important role in the realization of bulk heterojunction (BHJ) polymer solar cells (PSCs) with high efficiency as an economically viable source of renewable energy[1–4] and organic field-effect transistor (OFET) with high mobility to apply in display technology.[5,6] Combination of an electron-donating (D) unit with an electron-accepting (A) heterocycle along the polymer backbone has been proven to be an effective strategy to exploit new low band-gap conjugated polymer.[7,8] Generally, the highest occupied molecular orbital (HOMO) energy level of a D–A copolymer is mainly determined by D-type moiety and its lowest unoccupied molecular orbital (LUMO) energy level is dominantly attributed to A-type moiety.[9–11] As a consequence, alternating hybridization of a strong D-type unit and a strong A-type unit could give rise to narrow band gap D–A copolymer to match solar spectrum and then could achieve high current. Moreover, the D–A conjugated structure is also benefit to achieve a high mobility.[5,12–14] Planar polycyclic aromatics are favored to be as D-type units because of their good planarity and extended π-conjugated length, which are beneficial for π–π stacking between polymer main chain, charge separation, and transport as well as tunable energy levels. One of the famous tricyclic aromatic rings is benzodithiophene (BDT) unit, which has been attracted a great deal of attention. BHJ PSCs with BDT-based copolymers as the polymer donors have shown high power conversion efficiencies (PCEs) over 8%.[15–23] In addition to the tricyclic ring system, the larger π-conjugated tetracyclic aromatics are also of great interest to researchers. For instance, Peng's group[24] synthesized the copolymer based on naphthodithiophene (NDT), a tetracyclic donor unit, and achieved high efficiency of 6.92%.

With the success example of NDT, the property of new polycyclic aromatic ring is greatly encouraged to be studied. Several groups focus on the opto-electronic performance based on pentacyclic aromatic ring, among which the anthradithiophene (ADT) unit has been investigated as a building block

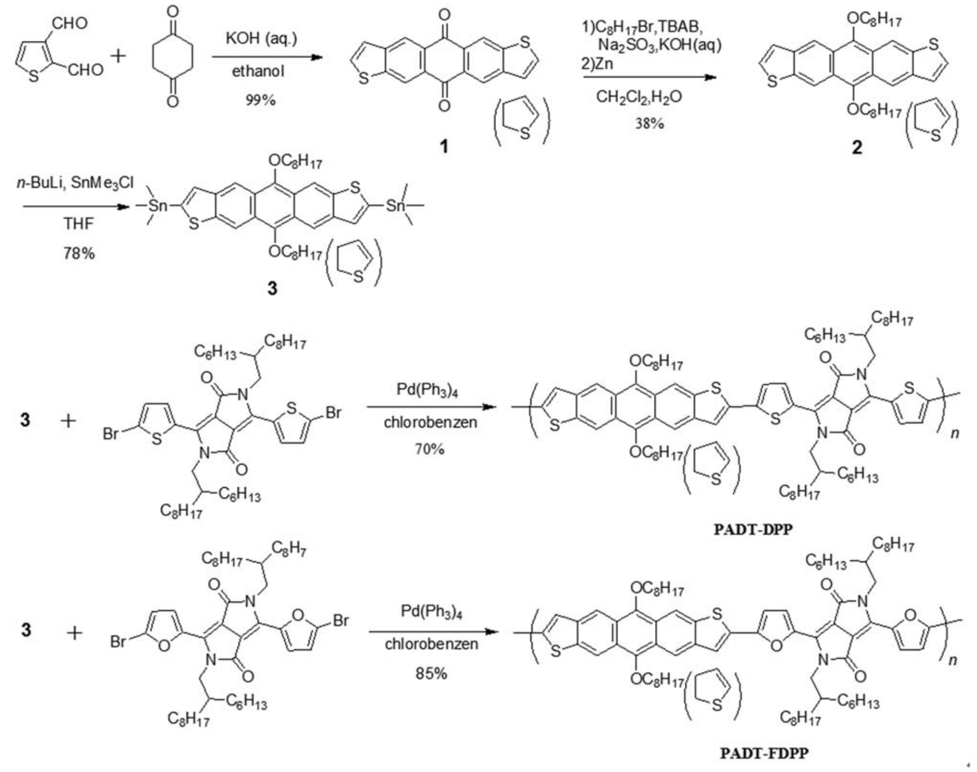

SCHEME 1 Synthesis routes for polymers PADT-DPP and PADT-FDPP.

of small molecular semiconducting materials for OFETs[25–29] and photovoltaic cells.[25,30–32] Katz group[28] first reported the field-effect mobilities of ADT-based small molecules, which were in the range of 0.01–0.02 $cm^2/(V\ s)$. Recently, the hole mobility of ADT-based small molecule was achieved as high as 5.4 $cm^2/(V\ s)$ by Anthony and Jurchescu[29] through the replacement of a trialkylsilyl substituent with a trialkylgermyl group. Malliaras's group[25] modified the structure of triethylsilyl ADT-based donor for solar cells and the resulting PCE was only 1%. It is of interest to introduce ADT as a building block for novel conjugated polymers. In a report by Bao's group,[30] two ADT-based copolymers comprising cyclopentadithiophene and dialkylfluorene were synthesized. The two polymers showed OFET hole mobility as high as 0.01 $cm^2/(V\ s)$, however, the highest PCE in BHJ solar cells was merely 0.94%. Furthermore, Bao's group[31] reported a conjugated copolymer based on 5,11-diethynyl-ADT and diketopyrrolopyrrole. The polymer exhibited enhanced thin-film order and high OFET hole mobility of 0.1 $cm^2/(V\ s)$ was achieved. Recently, Choi's group[32] reported a group of ADT-based copolymers. The alternating copolymer based on ADT and thieno[3,4-*b*]thiophene (TT) displayed a not high PCE of 1.5% in a solar cell, obviously lower than those achieved with terpolymers based on ADT, BDT, and TT. So far, it is a challenging work to realize an efficient solar cell with ADT-based alternating copolymer.

In this work, two new ADT-based conjugated copolymers with a D–A alternating skeleton were designed, in which the ADT was used as the D-unit and diketopyrrolopyrrole as A-unit (Scheme 1). The diketopyrrolopyrrole core is widely considered as a strong acceptor, which has exhibited great potential in polymer materials of high efficiency[8] or high OFET mobility.[5] The two ADT-based polymers, named as PADT-DPP and PADT-FDPP, comprised thiophene and furan as the π-conjugated bridges, respectively, so as to study the spacer effect of heterocycles in the conjugated polymers. PADT-DPP and PADT-FDPP exhibit broad absorption bands with absorption edges more than 825 nm. The two polymers possessed OFET hole mobilities of 10^{-3} $cm^2/(V\ s)$. When measured by space-charge-limited current (SCLC) method, the two polymers exhibited hole mobilities at a level of 10^{-4} $cm^2/(V\ s)$, suggesting fairly good hole transport property. With the polymers as donors in BHJ solar cells, PCEs up to 3.46% were achieved.

EXPERIMENTAL

Materials

All reagents solvents, unless otherwise specified, were obtained from Aldrich, Acros, and TCI Chemical and were used as received. Anhydrous tetrahydrofuran was distilled over sodium/benzophenone under N_2 prior to use. All manipulations involving air-sensitive reagents were performed under an atmosphere of dry argon. 3,6-Bis(5-bromothien-2-yl)-2,5-bis(2-octyldodecanyl)pyrrolo[3,4-*c*]pyrrole-1,4(2H,5H)-dione (DPP) and 3,6-bis(5-bromofuran-2-yl)-2,5-bis(2-octyldodecanyl)pyrrolo[3,4-*c*]pyrrole-1,4(2H,5H)-dione (FDPP) were prepared similarly according to literatures.[33,34]

Instrumentations

^{1}H NMR spectra were recorded on a Bruker AV 300 spectrometer with tetramethylsilane (TMS) as the internal reference. Molecular weights of the polymers were obtained on a Waters GPC 2410 using a calibration curve of polystyrene standards, with tetrahydrofuran as the eluent. Elemental analyses were performed on a Vario EL elemental analysis instrument (Elementar). UV–vis absorption spectra were recorded on an HP 8453 spectrophotometer. Cyclic voltammetry was performed on a CHI660A electrochemical work station with platinum electrodes at a scan rate of 50 mV/s against an Ag/Ag$^+$ reference electrode with a nitrogen-saturated solution of 0.1 M tetrabutylammonium hexafluorophosphate (Bu_4NPF_6) in acetonitrile. Potentials were referenced to the ferrocenium/ferrocene couple using ferrocene as an internal standard. The deposition of a copolymer on the electrode was done by the evaporation of a dilute THF solution. Tapping-mode atomic force microscopy (AFM) images were obtained using a Nano Scope NS3A system (Digital Instrument) to observe the surface morphology of active layers of polymer/$PC_{71}BM$ blends.

1,7-Dithia-dicyclopenta[b,i]anthracene-5,11-dione (1)

1,4-Cyclohexanedione (0.84 g, 7.5 mmol) was added to a solution of 2,3-thiophene dicarbaldehyde (2.1 g, 15 mmol) in ethanol (100 mL). Fifteen percentage of potassium hydroxide solution (6 mL) was added dropwise and then precipitate was formed. After stirred for 4 h at room temperature, the light yellow precipitate was obtained by filtration and washed several times by ethanol in 99% yield, without further purification for next step.

5,11-Bis(octyloxy)anthra[2,3-b:6,7-b′]dithiophene (2)

Compound **1** (0.5 g, 1.56 mmol), sodium hyposulfite (2.71 g, 15.6 mmol), and tetrabutylammonium bromide (0.08 g, 0.25 mmol) were put into a 50 mL flask. Under the protection of nitrogen, 20 mL CH_2Cl_2 and 5 mL H_2O were added by syringe. After stirred for 15 min, potassium hydroxide (1.74 g, 31.2 mmol) in 3 mL water was added dropwise. Keeping stirring for 5 min, 1-bromooctane (3.9 g, 15.6 mmol) was added in one portion. The mixture was stirred at room temperature for 5 h, and zinc powder (0.51 g, 7.8 mmol) was added carefully. Then, the reaction solution was refluxed at 50 °C for 3 days. The reactant was extracted by 150 mL CH_2Cl_2 and dried with $MgSO_4$. After removing the solvent in vacuum, purification was performed via silica gel column chromatography, using CH_2Cl_2:petroleum ether = 1:4 as the eluent. Red solid (0.39 g) of compound **2** was obtained in 38% yield.

^{1}H NMR ($CDCl_3$, 300 MHz), δ (ppm): 8.81 (s, 4H), 7.49 (d, 2H), 7.42 (d, 2H), 4.26 (t, 4H), 2.15 (t, 4H), 1.72 (t, 4H), 1.54–1.22 (m, 32H), 0.88 (t, 6H). ^{13}C NMR ($CDCl_3$, 75 MHz), δ (ppm): 138.80, 137.70, 129.02, 128.91, 125.19, 123.75, 123.01, 116.61, 115.29, 63.09, 32.80, 31.90, 31.79, 30.76, 29.59, 29.38, 29.26, 26.27, 25.72, 22.70, 14.13.

5,11-Bis(octyloxy)-2,8-bis(trimethyltin)anthra[2,3-b:6,7-b′]dithiophene (3)

Compound **2** (300 mg, 0.46 mmol) was dissolved into 40 mL fresh THF under the nitrogen. The mixture was cooled to −78 °C, then n-BuLi (2.5 M in THF, 1.1 mmol) was added dropwise into the solution. Keeping the mixture stirring at −78 °C for 1 h, then warmed to room temperature and stirred for another 1 h. A Me_3SnCl (1 M in THF, 1.1 mmol) solution was added in one portion at −78 °C. The mixture was kept at −78 °C for 1 h and then stirred for overnight. Subsequently, 10 mL water was added, and extracted with CH_2Cl_2. Then, the organic layer was dried over $MgSO_4$ and concentrated by vacuum. The crude product was recrystallized by ethanol two times and finally afforded red-needle crystals (353 mg, 78%).

^{1}H NMR ($CDCl_3$, 300 MHz), δ (ppm): 8.78 (d, 4H), 7.50 (s, 2H), 4.24 (t, 4H), 2.12 (t, 4H), 1.71 (t, 4H), 1.71–1.28 (m, 32H), 0.88 (t, 6H), 0.48 (s, 18H). ^{13}C NMR ($CDCl_3$, 75 MHz), δ (ppm): 146.82, 144.87, 144.72, 141.44, 141.27, 140.02, 139.94, 131.82, 123.08, 122.66, 122.32, 115.38, 114.20, 31.95, 30.78, 29.75, 29.70, 29.40, 26.30, 22.72, 14.15, −8.44.

Polymerization

Both of the two polymers were performed by palladium(0)-catalyzed Stille polycondensation reactions with equivalently molar ratio of a bis(trimethylstannyl)-substituted monomer to the dibromo monomer under argon protection. The purification of the polymers was conducted in air. The preparation of PADT-DPP and PADT-FDPP was performed according to the same procedures as follows.

Polymer PADT-DPP

Compound **3** (200 mg, 0.229 mmol) and 3,6-bis(5-bromothien-2-yl)-2,5-bis(2-hexyldecanyl)pyrrolo[3,4-*c*]pyrrole-1,4(2H,5H)-dione (DPP) (207 mg) were dissolved in a mixture of 12 mL chlorobenzene and 2 mL DMF in a flask under argon. The solution was flushed by argon for 20 min, then $Pd(PPh_3)_4$ (5%) was added. After 20 min flushed by argon, the reaction mixture was heated to 120 °C slowly. The solution was stirred for 24 h under argon atmosphere. Then, the solution was cooled down to room temperature and poured into 500 mL methanol. The precipitated solid was placed in a Soxhlet thimble, and extracted consecutively with methanol, ethyl acetate, and chlorobenzene. The chlorobenzene fraction was concentrated and poured into methanol. The title polymer was obtained as dark green solid and the yield was 70%. High temperature gel permeation chromatography (GPC) (1,2,4-trichlorobenzene, 140 °C): M_n 38.7 kg/mol; M_w/M_n 3.14 (Table 1). ELEM. ANAL. calcd. for $(C_{80}H_{112}N_2O_4S_4)_n$: C, 71.44; H, 8.26; N, 2.06. Found: C, 74.25; H, 8.72; N, 2.16. The solubility of the polymer in deuterated chloroform or deuterated *o*-dichlorobenzene was too low to obtain reliable NMR data.

Polymer PADT-FDPP

This polymer was synthesized as the same procedure of PADT-DPP, using 3,6-bis(5-bromofuran-2-yl)-2,5-bis(2-hexyldecanyl)pyrrolo[3,4-*c*]pyrrole-1,4(2H,5H)-dione (FDPP) as the dibromo monomer and the yield was 85%. High temperature GPC (1,2,4-trichlorobenzene, 140 °C): M_n 30.2 kg/mol; M_w/M_n 4.12 (Table 1). ELEM. ANAL. calcd. for $(C_{80}H_{112}N_2O_6S_2)_n$: C, 75.70; H, 8.56; N, 2.26. Found: C, 76.14; H, 8.95; N, 2.22.

TABLE 1 Polymerization Yields, Molecular Weights, and Decomposition Temperatures of PADT-DPP and PADT-FDPP

Polymer	Yield (%)	M_n[a] (kg/mol)	M_w/M_n[a]	T_d (°C)[b]
PADT-DPP	70	38.7	3.14	319
PADT-FDPP	85	30.2	4.12	298

[a] Estimated by GPC at 150 °C with 1,2,4-trichlorobenzene as the eluent.
[b] Temperature for 5% weight loss measured by TGA at a heating rate of 20 °C/min under nitrogen.

The solubility of the polymer in deuterated chloroform or deuterated *o*-dichlorobenzene was too low to obtain reliable NMR data.

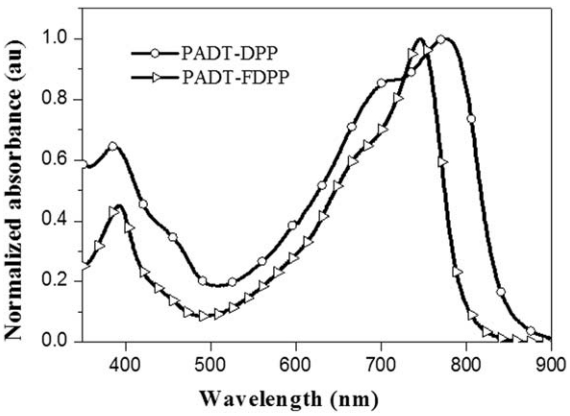

FIGURE 2 UV absorption spectra of PADT-DPP and PADT-FDPP in chlorobenzene.

Fabrication and Charaterization of Solar Cells

Patterned indium tin oxide (ITO)-coated glass with a sheet resistance of 15−20 ohm/square was cleaned by a surfactant scrub and then underwent a wet-cleaning process inside an ultrasonic bath, beginning with deionized water, followed by acetone and 2-propanol. After oxygen plasma cleaning for 5 min, a 40-nm-thick poly(3,4-ethylenedioxythiophene):poly(styrenesulfonate) (PEDOT:PSS) (Bayer Baytron 4083) anode buffer layer was spin-cast onto the ITO substrate and then dried by baking in a vacuum oven at 80 °C overnight. The active layer based on ADT-based polymer: $PC_{71}BM$ = 1:2, with a thickness of 85 nm, was then deposited on top of the PEDOT:PSS layer, by casting from a chlorobenzene solution, and drying at 70 °C for 10 min. A DMF solution of PC-EP was spin-coated on the top of the active layer and dried at 120 °C for 10 min to form a thin cathode interlayer of 10 nm. The thickness of the PEDOT:PSS and the active layer was verified by a surface profilometer (Tencor, Alpha-500). Determination of the thickness of the interlayer followed a previously published paper.[10] Finally, a 100 nm aluminum layer was evaporated with a shadow mask. The overlapping area between the cathode and the anode defined a pixel size of 0.16 cm^2. Except for the deposition of the PEDOT:PSS layers, all the fabrication processes were performed inside a controlled atmosphere of nitrogen dry box (Vacuum Atmosphere) containing less than 10 ppm oxygen and moisture. The power conversion efficiencies of the resulting polymer solar cells were measured under 1 sun, AM 1.5G (air mass 1.5 global) spectrum from a solar simulator (Oriel model 91192) 100 mW/cm^2. The current density−voltage ($J-V$) characteristics were recorded with a Keithley 2410 source unit. The external quantum efficiencies of the conventional solar cells were measured with a commercial photo modulation spectroscopic setup, including a xenon lamp, an optical chopper, a monochromator, and a lock-in amplifier operated by a PC computer, and a calibrated Si photodiode was used as a standard.

FET Fabrication and Characterization

To measure the hole mobilities of the polymers, FETs were fabricated in a top contact geometry using silver as the source and drain electrode. Highly *n*-doped silicon and thermally grown silicon dioxide (300 nm) were used as the back gate and gate dielectric, respectively. Octyltrichlorosilane (OTS) was then used for surface modification of the gate dielectric layer. The copolymers films (60 nm) were spin-coated on OTS treated substrates from chlorobenzene solution (18 mg/mL) at 2000 rpm, and then annealed at 100 °C

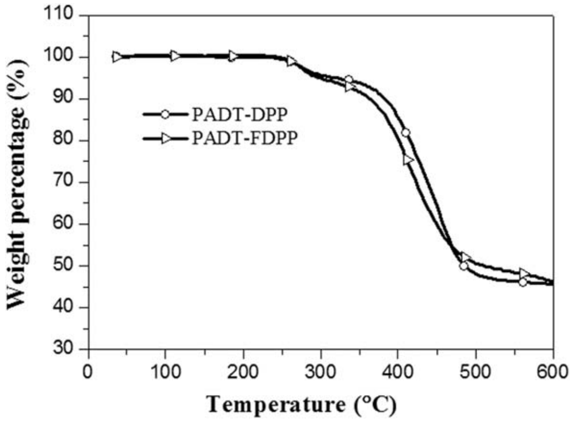

FIGURE 1 TGA curves of PADT-DPP and PADT-FDPP with a heating rate of 20 °C/min under nitrogen.

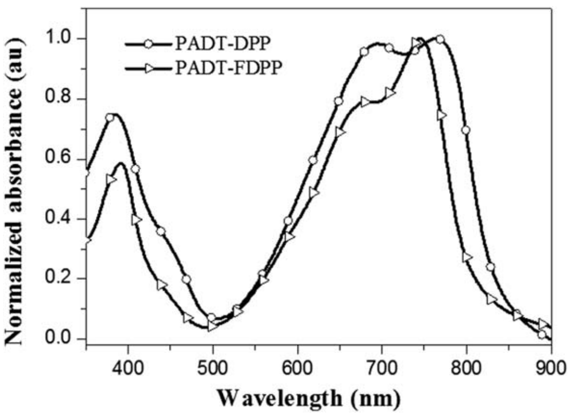

FIGURE 3 UV absorption spectra of PADT-DPP and PADT-FDPP films.

TABLE 2 Absorption Maxima, Optical Band Gaps, and Electrochemical Properties of the PADT-DPP and PADT-FDPP

Polymer	$\lambda_{\text{max-sol}}$[a] (nm)	$\lambda_{\text{max-film}}$[b] (nm)	E_g[c] (eV)	E_{ox} (V)	HOMO[d] (eV)	LUMO[e] (eV)
PADT-DPP	775	767	1.44	0.23	−5.03	−3.59
PADT-FDPP	745	751	1.50	0.36	−5.16	−3.66

[a] Chlorobenzene solutions.

[b] Thin solid film casted from chlorobenzene.

[c] Optical band gap estimated with the absorption edge of thin solid film.

[d] Calculated according to HOMO = $-e(E_{ox}+4.8)$.

[e] Calculated from the HOMO and optical band gap.

for 10 min. Then silver film (50 nm) was deposited under vacuum as the source and drain electrodes. The width to length ratio (W/L) of the FET devices is 100/1. The OFETs characterizations were performed in the atmosphere using a probe station and a semiconductor parameter analyzer (Agilent 4155C). Then field-effect mobility was calculated from the standard equation for saturation region in metal-dioxide-semiconductor field effect transistors: $I_{DS} = (W/2L)\mu C_i(V_G - V_T)^2$, where I_{DS} is the drain-source current, μ is the field-effect mobility, W and L are the channel width and length, C_i is the capacitance per unit area of the dielectric layer (C_i = 11 nF/cm^2), V_G is the gate voltage, and V_T is the threshold voltage.

SCLC Measurement

Hole-only devices were fabricated to measure the hole mobility using SCLC method with a device configuration of ITO/PEDOT:PSS/Copolymer:PC$_{71}$BM/MoO$_3$/Al. The mobility was determined by fitting the dark current to the model of a single carrier SCLC, described by the equation:

$$J=\frac{9}{8}\varepsilon_0\varepsilon_r\mu_h\frac{V^2}{d^3},$$

where J is the current density, μ_h is the mobility under zero field, ε_0 is the permittivity of free space, ε_r is the material relative permittivity, d is the active layer thickness, and V is the effective voltage. The effective voltage can be obtained by subtracting the built-in voltage (V_{bi}) and the voltage drop (V_s) from the substrate's series resistance from the applied voltage (V_{appl}), $V = V_{appl} - V_{bi} - V_s$. The hole-mobility can be calculated from the slope of the $J^{1/2}-V$ curves.

RESULTS AND DISCUSSION

Synthesis of Monomers and Polymers

As depicted in Scheme 1, the bis(trimethylstannyl)anthradithiophene monomer **3** could be easily synthesized by three steps that were reported by Choi and coworkers.[32] We modified some of the procedures, from which higher yields could be achieved. For the step one, 1,4-cyclohexanedione and 2,3-thiophene dialdehyde were underwent a cyclization reaction for a longer time of 4 h under the basic condition (15% KOH solution), which formed the dione compound **1** with a perfect yield of 99%. It should be noted that there were two isomers of compound **1** mixed together and it was difficult to separate them from each other.[25,28] However, in previous reports, ADT-based small molecules of isomer nature could exhibit high hole mobility up to 5.4 cm^2/(V s).[29] Then the dione compound **1** was reacted with sodium hyposulfite, followed by alkylation of 1-bromooctane to afford the dioctoxy compound **2**. It is worth noting that the subsequent use of zinc dust as the second reductant can result in a modified yield of 38%. In the last step, the monomer **3** could be readily afforded, and the pure powder of monomer **3** was obtained in a good yield of 78%, after twice recrystallized from ethanol.

The DPP and FDPP monomers were prepared according to those in literatures.[33,34] Two 2-hexyl dodecanyl side chains of a branched structure were attached on the diketopyrrolopyrrole unit so as to impart the target polymers with enough solubility. The alternating copolymers PAD-DPP and PADT-FDPP were performed by palladium(0)-catalyzed Stille polycondensation reactions (Scheme 1) and their corresponding polymerization yields are summarized in Table 1, with the values of 70% and 85%, respectively.

Two polymers can be easily dissolved in warm chlorobenzene (CB) and *o*-dichlorobenzene. Their molecular weights were performed by GPC at 150 °C with 1,2,4-trichlorobenzene as the eluent (Table 1). The M_n values of PADT-DPP and PADT-FDPP are 38.7 and 30.2 kg/mol, with polydispersity index (M_w/M_n) of 3.14 and 4.12, respectively. Thermal stability was investigated by thermogravimetric analysis (TGA), as shown in Figure 1. PADT-DPP showed decomposition temperatures at 319 °C while PADT-FDPP has a slightly lower

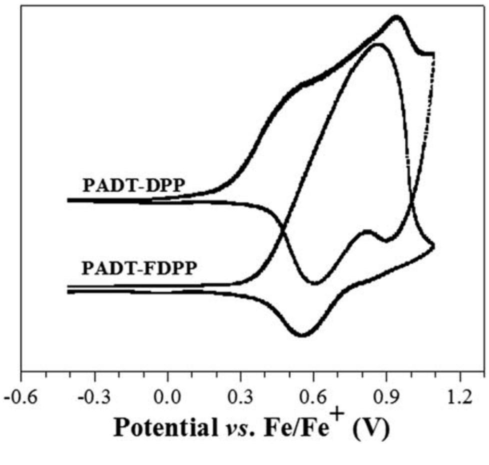

FIGURE 4 Cyclic voltammograms of PADT-DPP and PADT-FDPP films.

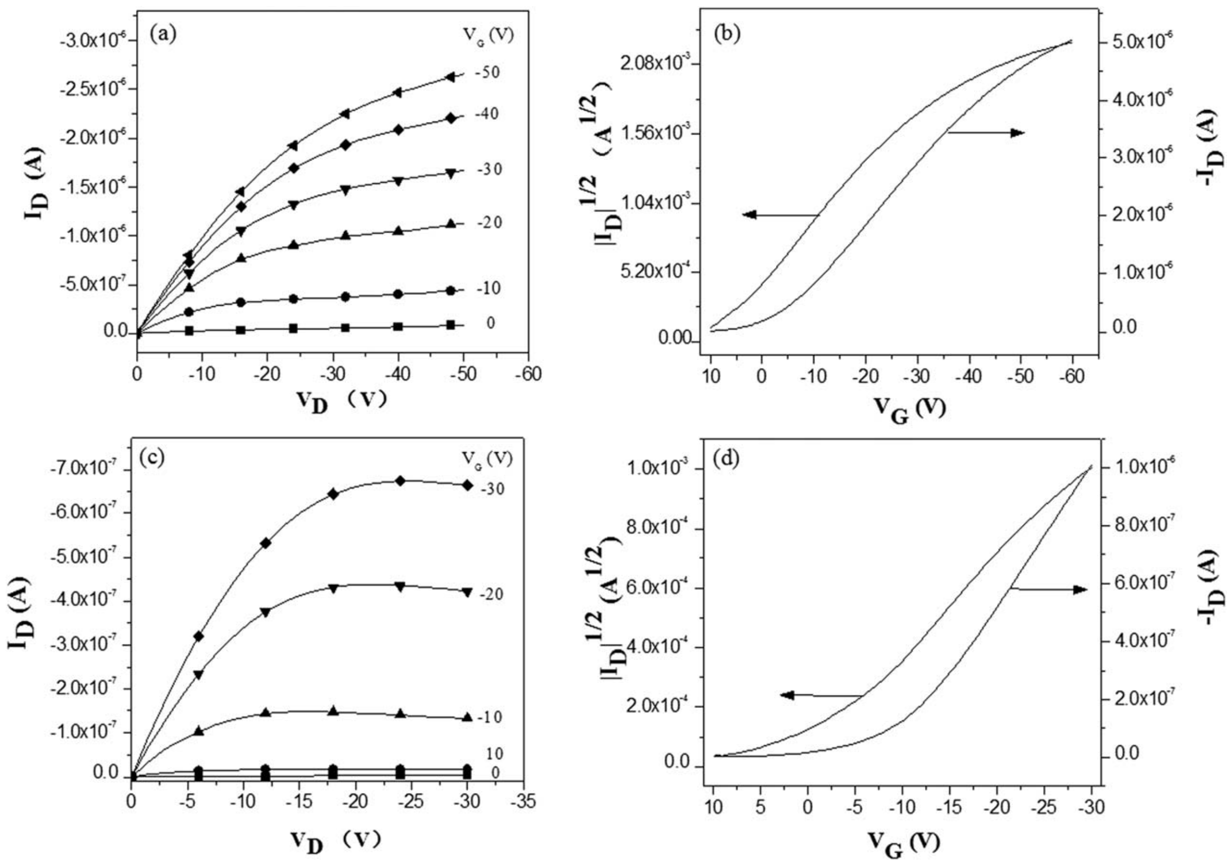

FIGURE 5 The FET output characteristics of (a) PADT-DPP and (c) PADT-FDPP and transfer characteristics of (b) PADT-DPP and (d) PADT-FDPP.

decomposition temperature at 298 °C. No peaks associated with crystallization/melting transitions of the polymers were detected by differential scanning calorimetry (DSC) analyses.

UV–Vis Absorption and Energy Level

The UV–vis absorption spectra of PADT-DPP and PADT-FDPP in CB solutions are shown in Figure 2. Both the polymers display two absorption bands, similar to many D–A conjugated copolymers. The peaks for the first band are located at 385 and 392 nm for PADT-DPP and PADT-FDPP, respectively. The second band at the long-wavelength range, with the absorptions peaks at 775 for PADT-DPP and 745 nm for PADT-FDPP, should be attributed to intramolecular charge transfer (ICT) of the D–A conjugated polymers.[24] The extent of ICT transition is an indirect parameter to assess the electron-donating ability of a donor unit.[35] The ratio of the maximum absorbance of the first band to the second band in PADT-DPP is 0.64, which is higher than that in PADT-FDPP with a value of 0.45. The results indicate that furan as spacer could enhance the electron-donating ability of the ADT unit in D–A copolymer, which in accordance with the electron-donating features on benzodifuran unit.[36]

The absorption spectra of polymer films are shown in Figure 3. In comparison to the absorptions in the CB solutions, the absorption peaks for the polymer films do not show obvious shifts. However, the films of the both polymers exhibit remarkably enhanced absorptions of shoulder peaks at 694 nm for PADT-DPP and 677 nm for PADT-FDPP. Overall, for the solution or the film, PADT-DPP with thiophene spacers can display a broader absorption of the second band than that of PADT-FDPP with furan spacers. The optical band gaps (E_g) for PADT-DPP and PADT-FDPP were calculated from the onset wavelengths of the film absorption spectra, which are 1.44 and 1.5 eV, respectively (Table 2).

The HOMO levels of the copolymers (Table 2) were obtained from the onsets of the oxidation potentials during the cyclic voltammetry (CV) measurement. The corresponding CV spectra are shown in Figure 4. Polymers PADT-DPP and PADT-FDPP showed reversible oxidations during the CV scans. The HOMO level of PADT-DPP is at −5.03 eV, while that of PADT-FDPP have a slightly lower HOMO level of −5.16 eV. The results indicate that the HOMO levels of the ADT-based polymers are mainly determined by the ADT unit and the thiophene spacers result in a higher HOMO level if compared with the furan spacers. The LUMO levels of the ADT-based copolymers are given from the corresponding optical band gaps and HOMO levels. The calculated LUMO level for PADT-DPP is at −3.59 eV, which is slightly higher than that of PADT-FDPP (−3.66 eV).

TABLE 3 OFET Hole Mobilities and Space-Charge-Limited Current Mobilities of PADT-DPP and PADT-FDPP

Polymer	μ_{FET} [cm^2/(V s)]	μ_{SCLC} [cm^2/(V s)]
PADT-DPP	4.7×10^{-3}	4.98×10^{-4}
PADT-FDPP	2.7×10^{-3}	4.40×10^{-4}

Field-Effect Transistor and SCLC Measurement

Several ADT-based small molecules have exhibited high hole mobilities in OFETs.[27,29] To measure OFET hole mobilities of PADT-DPP and PADT-FDPP, we fabricated OFET devices with a top contact configuration, where PADT-DPP or PADT-FDPP film (60 nm) was spin-coated on an octyltrichlorosilane (OTS)-treated SiO_2 gate insulator. The polymer films were dried at 100 °C for 10 min and then silver film (50 nm) was deposited under vacuum as the source and drain electrodes. The width to length ratio (W/L) of the FET devices is 100/1. The main reason for using silver as the electrode metal is due to its great potential in printable electronics: solution-processable silver nanoparticle ink can be sintered at a low temperature of 100 °C or less.[37] Moreover, silver is a much cheaper metal than gold, a widely used electrode metal for OFET devices. In a recent report, an excellent polymer hole mobility of 1.92 cm^2/(V s) was achieved in OFET devices with silver electrodes.[38]

The output and transfer characteristics of the OFETs are shown in Figure 5. At different gate voltages (V_G), the drain current (I_D) of the devices could reach saturation along with the drain voltage (V_D) [Fig. 5(a,c)]. From the slopes of the curves of $(I_D)^{1/2}$ versus V_G [Fig. 5(b,d)], the calculated hole mobilities (μ_{FET}) are 4.7×10^{-3} and 2.7×10^{-3} cm^2/(V s) for PADT-DPP and PADT-FDPP, respectively (Table 3), and the corresponding on/off current ratios both are 1×10^3. The somewhat low on/off current ratios of the OFET devices may be related to the silver source and drain electrodes, which may result in contact resistance due to its lower work function than that of gold. The μ_{FET} values of PADT-DPP and PADT-FDPP also suggest that the thiophene spacers can supply a higher mobility in the resulting ADT-based polymer if compared with the furan spacers.

ADT-based small molecules have exhibited high hole mobility up to 5.4 cm^2/(V s)[29] because of the forming of ordered film. Relatively, the much lower μ_{FET} values for PADT-DPP and PADT-FDPP in this work imply that the films of PADT-DPP and PADT-FDPP are of poor order. Fine tuning of the side chains of the ADT-based polymers would be useful to improve their hole mobilities.

OFET performance largely relies on the lateral mobility of a semiconducting film. However, carrier transport in polymer solar cells is more related to the transportation in vertical direction, which could be obtained by SCLC. Hole-only devices were fabricated to measure the SCLC hole mobility (μ_{SCLC}) for the pristine polymer films (Fig. 6). The resulting data are listed in Table 3. PADT-DPP shows a μ_{SCLC} of 4.98×10^{-4} cm^2/(V s), slightly higher than that of 4.40×10^{-4} cm^2/(V s) for PADT-FDPP, indicating that the two polymers are fairly good for the charge transport in polymer solar cells.

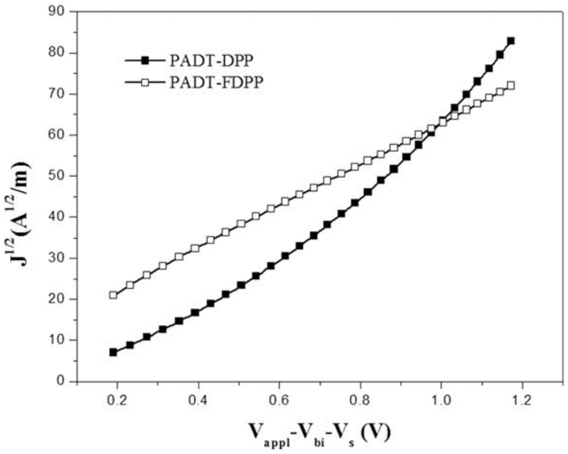

FIGURE 6 SCLC curves of the hole-only devices based on pristine films of PADT-DPP and PADT-FDPP.

Photovoltaic Performance

Bilayer cathode consisting of a hydrophilic conjugated polymer and a high work-function metal electrode has shown great potential to improve the device performances, where open-circuit voltage (V_{oc}), short-circuit current density (J_{sc}), and fill factor (FF) could be increased simultaneously in some cases.[10,39] 2,7-Carbazole-1,4-phenylene-based alternating copolymer (PCP-EP) with phosphonate end groups as pendants has exhibited good modification effects as cathode interlayer in light-emitting diodes and solar cells.[35,40] Here, we also selected the PCP-EP/Al as the bilayer cathode for the constructions of solar cells with a device configuration of ITO/PEDOT:PSS (40 nm)/(polymer:$PC_{71}BM$ = 1:2) (80 nm)/PCP-EP (10 nm)/Al (100 nm). The blend ratio of 1:2 for the active layer could show the best efficiency for the two D–A polymers PADT-DPP and PADT-FDPP.

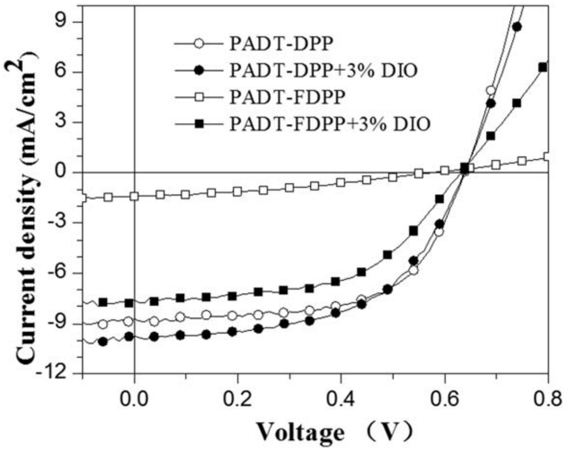

FIGURE 7 *J–V* characteristics of polymer solar cells as measured under illumination of AM 1.5G simulated solar light at 100 mW/cm^2.

TABLE 4 Photovoltaic Parameters of Polymer Solar Cells Based on PADT-DPP and PADT-FDPP as Measured Under Irradiation of AM 1.5G at 100 mW/cm^2

Polymer	DIO	V_{oc} (V)	J_{sc} (mA/cm^2)	FF (%)	PCE^a (%)
PADT-DPP	No	0.64	8.73	61.6	3.44 (3.33)
	3%	0.64	9.74	55.5	3.46 (3.37)
PADT-FDPP	No	0.57	1.44	35.3	0.29 (0.26)
	3%	0.63	7.61	54.6	2.62 (2.56)

[a] Data in the parentheses are the averaged values based on over five devices.

The measurements of the photovoltaic performances of the ADT-based copolymers as donors in the BHJ PSCs were performed under illumination of AM 1.5G simulated solar light at 100 mW/cm^2. The current density–voltage (J–V) characteristics of the BHJ PSCs are shown in Figure 7. Their solar cell parameters are listed in Table 4. The device based on polymer PADT-DPP exhibited a not high open-circuit voltage (V_{oc}) of 0.64 V, which was generally agreement with its HOMO level. The measured short-circuit current (J_{sc}) and fill factor (FF) of the device were 8.73 mA/cm^2 and 61.6%, respectively. The resulting PCE of 3.44% was achieved. The average PCE for PADT-DPP was 3.33%. The device based on PADT-FDPP showed a lower V_{oc} of 0.57 V, a very bad J_{sc} of 1.44 mA/cm^2, and a low FF of 35.3%, giving a very poor PCE of 0.29%. The first furan-based D–A copolymer in the report by Fréchet et al.[34] also suffered from a low PCE of 0.86% (PC$_{71}$BM as the acceptor), but a solvent additive could improve its efficiency by more than fivefold. In this work, we used 1,8-diiodooctane (DIO) as the additive and the corresponding results were also listed in the Table 4. As expected, the performance of PADT-FDPP-based device can be improved greatly, with an elevated V_{oc} of 0.63 V, a larger J_{sc} of 7.61 mA/cm^2, and a higher FF of 54.6%, so the resulting PCE (2.62%) is improved by ninefold. Nevertheless, the photovoltaic performance of PADT-DPP was practically not changed in the presence of the DIO additive because of unchanged V_{oc}, slightly increased J_{sc}, and slightly decreased FF. We tried 1-chloronaphthalene (CN) as the solvent

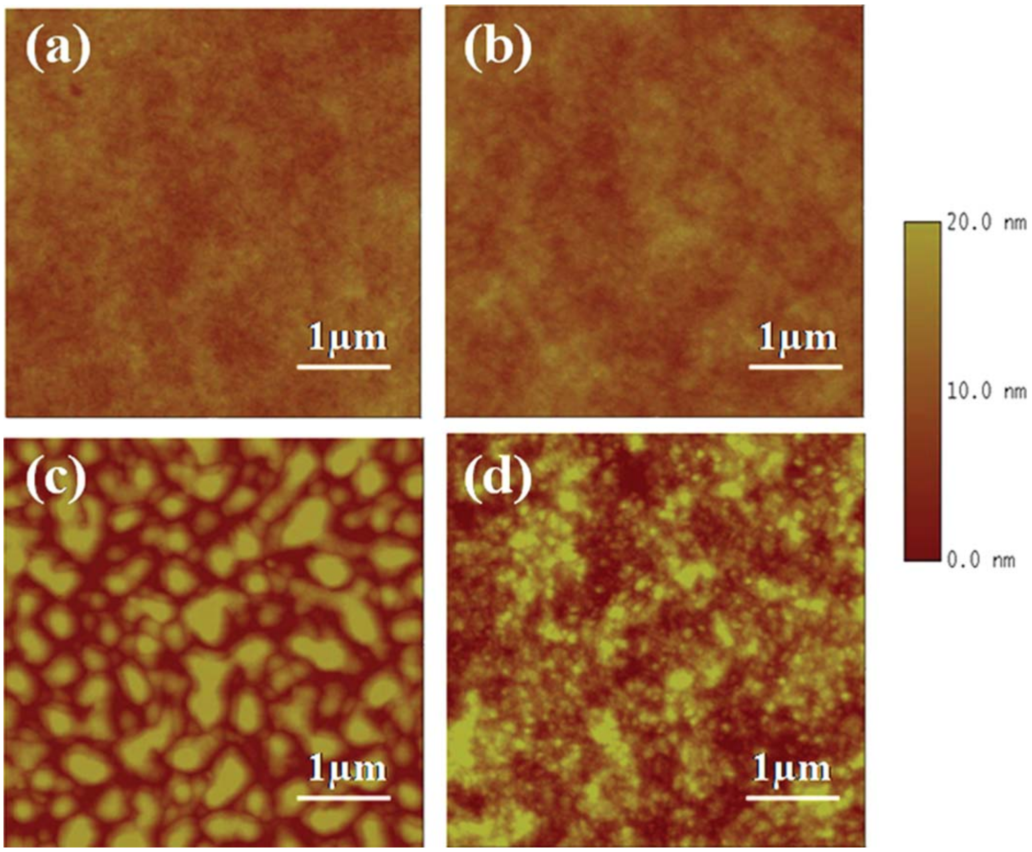

FIGURE 8 Tapping-mode AFM images of (a) PADT-DPP, (b) PADT-DPP+3% DIO, (c) PADT-FDPP, and (d) PADT-FDPP+3% DIO films.

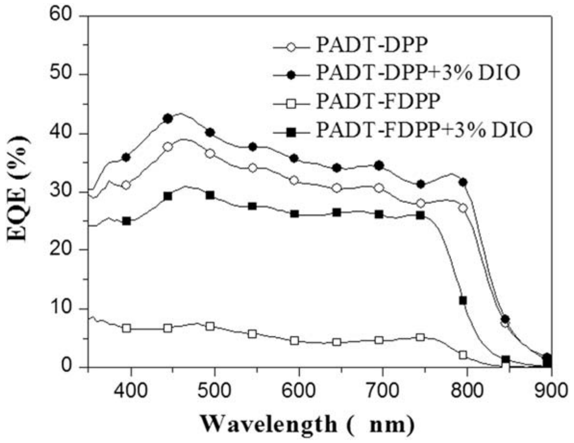

FIGURE 9 EQE curves of the polymer solar cells.

additive. Unfortunately, lower photovoltaic performances than those with DIO were found.

Further insight into the microstructure of the active layer, it is essential to explore the morphology of blend film. AFM was applied to reveal the morphology of active layer surface. The AFM topographic images of the blend film are shown in Figure 8. For PADT-DPP-based blend films, the morphology fabricated without DIO [Fig. 8(a)] is very close to that with 3% DIO [Fig. 8(b)], which is in good agreement with the corresponding photovoltaic performance with DIO as the solvent additive. As shown in Figure 8(c), the domain size of the blend film based on PADT-FDPP and $PC_{71}BM$ is very large, which is detrimental to charge separation and transport. With 3% DIO as the solvent additive, the former island shape morphology of PADT-FDPP disappears [Fig. 8(d)], and a pattern of fairly continuous phase separation emerges, from which the efficiency can be greatly improved. The morphology study indicates that the polymer containing furan spacer needs the assistance of a solvent additive to deposit the blend film, so as to form a better interpenetrating network toward good charge separation and transport.

The external quantum efficiency (EQE) curves of the solar cells are shown in Figure 9. Without the DIO, the maxima of the two EQE curves are within 38.9% and 8.4% for PADT-DPP and PADT-FDPP, respectively. With the DIO, the EQE maximum of PADT-DPP is slightly increased to 43.1% that can match the slight increasing of J_{sc}. As expected, the PADT-FDPP-based solar cell with 3% DIO shows an EQE maximum of 30.9%, well reflecting the obviously modified J_{sc}. Generally, the wide EQE characteristics of the solar cells follow the wavelength range of the UV–vis absorption spectra of the ADT-based copolymers, where $PC_{71}BM$ absorption to solar light also obviously contributes to the EQE curves.

CONCLUSIONS

In summary, the two anthradithiophene-based copolymers PADT-DPP and PADT-FDPP, with thiophene and furan as the π-conjugated bridge, respectively, were successfully synthesized, and both of them exhibited broad absorption bands with optical band gaps of 1.44 and 1.50 eV, respectively. Their HOMO levels are between -5.03 and -5.16 eV. PADT-DPP and PADT-FDPP displayed OFET hole mobilities of 4.7×10^{-3} and 2.7×10^{-3} $cm^2/(V\ s)$, respectively, while their SCLC hole mobilities were 4.98×10^{-4} and 4.40×10^{-4} $cm^2/(V\ s)$, respectively. PADT-DPP showed obviously higher PCE of 3.44% than the 0.29% for PADT-FDPP. The poor efficiency of PADT-FDPP should be related to the island-shaped morphology of its active layer. DIO as the solvent additive did not contribute to the PCE of PADT-DPP due to very limited morphology changing. However, the addition of DIO could remarkably elevate the PCE PADT-FDPP to 2.62% because of the obviously improved two-phase separation. These efficiencies are higher than those of the previously reported anthradithiophene-based conjugated polymers, suggesting the anthradithiophene as an electron-donating polycyclic system is useful to construct new D–A alternating copolymers for efficient polymer solar cells.

ACKNOWLEDGMENTS

The authors gratefully acknowledge the financial support of National Natural Science Foundation of China (Nos. 21225418 and 51173048), National Basic Research Program of China (973 program Nos. 2013CB834705 and 2014CB643505), Doctoral Fund of Ministry of Education of China (20120172110008), and GDUPS (2013).

REFERENCES AND NOTES

1 S. Günes, H. Neugebauer, N. S. Sariciftci, *Chem. Rev.* **2007**, *107*, 1324–1338.

2 B. C. Thompson, J. M. J. Fréchet, *Angew. Chem. Int. Ed.* **2008**, *47*, 58–77.

3 Y. Li and Y. Zou, *Adv. Mater.* **2008**, *20*, 2952–2958.

4 G. Dennler, M. C. Scharber, C. J. Brabec, *Adv. Mater.* **2009**, *21*, 1323–1338.

5 J. D. Yuen, F. Wudl, *Energy Environ. Sci.* **2013**, *6*, 392–406.

6 J. Mei, Y. Diao, A. L. Appleton, L. Fang, Z. Bao, *J. Am. Chem. Soc.* **2013**, *135*, 6724–6746.

7 J. Chen, Y. Cao, *Acc. Chem. Res.* **2009**, *42*, 1709–1718.

8 C. Duan, F. Huang, Y. Cao, *J. Mater. Chem.* **2012**, *22*, 10416–10434.

9 J. Hou, M.-H. Park, S. Zhang, Y. Yao, L.-M. Chen, J.-H. Li, Y. Yang, *Macromolecules* **2008**, *41*, 6012–6018.

10 L. Zhang, C. He, J. Chen, P. Yuan, L. Huang, C. Zhang, W. Cai, Z. Liu, Y. Cao, *Macromolecules* **2010**, *43*, 9771–9778.

11 E. Zhou, S. Yamakawa, K. Tajima, C. Yang, K. Hashimoto, *Chem. Mater.* **2009**, *21*, 4055–4061.

12 H. Chen, Y. Guo, G. Yu, Y. Zhao, J. Zhang, D. Gao, H. Liu, Y. Liu, *Adv. Mater.* **2012**, *24*, 4618–4622.

13 M. J. Cho, J. Shin, S. H. Yoon, T. W. Lee, M. Kaur, D. H. Choi, *Chem. Commun.* **2013**, *49*, 7132–7134.

14 D. H. Lee, J. Shin, M. J. Cho, D. H. Choi, *Chem. Commun.* **2013**, *49*, 3896–3898.

15 Z. He, C. Zhong, X. Huang, W.-Y. Wong, H. Wu, L. Chen, S. Su, Y. Cao, *Adv. Mater.* **2011**, *23*, 4636–4643.

16 H.-C. Chen, Y.-H. Chen, C.-C. Liu, Y.-C. Chien, S.-W. Chou, P.-T. Chou, *Chem. Mater.* **2012**, *24*, 4766–4772.

17 S. Chen, C. E. Small, C. M. Amb, J. Subbiah, T.-H. Lai, S.-W. Tsang, J. R. Manders, J. R. Reynolds, F. So, *Adv. Energy Mater.* **2012**, *2*, 1333–1337.

18 Z. He, C. Zhong, S. Su, M. Xu, H. Wu, Y. Cao, *Nat. Photon.* **2012**, *6*, 591–595.

19 L. Lu, Z. Luo, T. Xu, L. Yu, *Nano Lett.* **2012**, *13*, 59–64.

20 S.-H. Liao, H.-J. Jhuo, Y.-S. Cheng, S.-A. Chen, *Adv. Mater.* **2013**, *25*, 4766–4771.

21 L. Lu, T. Xu, W. Chen, J. M. Lee, Z. Luo, I. H. Jung, H. I. Park, S. O. Kim, L. Yu, *Nano Lett.* **2013**, *13*, 2365–2369.

22 I. Osaka, T. Kakara, N. Takemura, T. Koganezawa, K. Takimiya, *J. Am. Chem. Soc.* **2013**, *135*, 8834–8837.

23 M. Zhang, Y. Gu, X. Guo, F. Liu, S. Zhang, L. Huo, T. P. Russell, J. Hou, *Adv. Mater.* **2013**, *25*, 4944–4949.

24 Q. Peng, Q. Huang, X. Hou, P. Chang, J. Xu, S. Deng, *Chem. Commun.* **2012**, *48*, 11452–11454.

25 M. T. Lloyd, A. C. Mayer, S. Subramanian, D. A. Mourey, D. J. Herman, A. V. Bapat, J. E. Anthony, G. G. Malliaras, *J. Am. Chem. Soc.* **2007**, *129*, 9144–9149.

26 K. C. Dickey, J. E. Anthony, Y. L. Loo, *Adv. Mater.* **2006**, *18*, 1721–1726.

27 M. M. Payne, S. R. Parkin, J. E. Anthony, C.-C. Kuo, T. N. Jackson, *J. Am. Chem. Soc.* **2005**, *127*, 4986–4987.

28 J. G. Laquindanum, H. E. Katz, A. J. Lovinger, *J. Am. Chem. Soc.* **1998**, *120*, 664–672.

29 Y. Mei, M. A. Loth, M. Payne, W. Zhang, J. Smith, C. S. Day, S. R. Parkin, M. Heeney, I. McCulloch, T. D. Anthopoulos, J. E. Anthony, O. D. Jurchescu, *Adv. Mater.* **2013**, *25*, 4352–4357.

30 Y. Jiang, T. Okamoto, H. A. Becerril, S. Hong, M. L. Tang, A. C. Mayer, J. E. Parmer, M. D. McGehee, Z. Bao, *Macromolecules* **2010**, *43*, 6361–6367.

31 Y. Jiang, J. Mei, A. L. Ayzner, M. F. Toney, Z. Bao, *Chem. Commun.* **2012**, *48*, 7286–7288.

32 Y. Lim, S.-G. Ihn, X. Bulliard, S. Yun, Y. Chung, Y. Kim, H. Chang, Y. S. Choi, *Polymer* **2012**, *53*, 5275–5284.

33 L. Huo, J. Hou, H.-Y. Chen, S. Zhang, Y. Jiang, T. L. Chen and Y. Yang, *Macromolecules* **2009**, *42*, 6564–6571.

34 C. H. Woo, P. M. Beaujuge, T. W. Holcombe, O. P. Lee, J. M. J. Fréchet, *J. Am. Chem. Soc.* **2010**, *132*, 15547–15549.

35 Z. Chen, P. Cai, L. Zhang, Y. Zhu, X. Xu, J. Sun, J. Huang, X. Liu, J. Chen, H. Chen, Y. Cao, *J. Polym. Sci., Part A: Polym. Chem.* **2013**, *51*, 4966–4974.

36 L. Huo, Y. Huang, B. Fan, X. Guo, Y. Jing, M. Zhang, Y. Li, J. Hou, *Chem. Commun.* **2012**, *48*, 3318–3320.

37 K. Fukuda, T. Sekine, Y. Kobayashi, D. Kumaki, M. Itoh, M. Nagaoka, T. Toda, S. Saito, M. Kurihara, M. Sakamoto, S. Tokito, *Org. Electron.* **2012**, *13*, 1660–1664.

38 Z. Chen, P. Cai, J. Chen, X. Liu, L. Zhang, L. Lan, J. Peng, Y. Ma, Y. Cao, *Adv. Mater.* **2014**, DOI: 10.1002/adma.201305092.

39 Z. He, C. Zhang, X. Xu, L. Zhang, L. Huang, J. Chen, H. Wu, Y. Cao, *Adv. Mater.* **2011**, *23*, 3086–3089.

40 X. Xu, B. Han, J. Chen, J. Peng, H. Wu, Y. Cao, *Macromolecules* **2011**, *44*, 4204–4212.